Neutron scattering study of the itinerant-electron magnet YMn_2

T. Freltoft, P. Böni, and G. Shirane
Physics Department, Brookhaven National Laboratory, Upton, New York 11973-5000

K. Motoya
Department of Physics, Faculty of Science, Saitama University, 255 Shimo-okubo, Urawa, Saitama 338, Japan
(Received 10 July 1987)

Neutron scattering with polarized beam analysis has been used to study the magnetic properties of the antiferromagnet YMn_2 ($T_N \simeq 100$ K). Previous susceptibility, NMR relaxation, and preliminary neutron measurements indicate a transition from a local-moment magnet in the ordered phase to an itinerant-electron magnet above T_N. We present a detailed analysis of magnetic-scattering data measured for temperatures ranging from $T=10$ K to $T=600$ K. The analysis includes energy integration of the paramagnetic response, simple model calculations of the measured powder average, and absolute calibration of the cross sections. The amplitude of the local magnetic moment per Mn atom is extracted and shown to drop by more than $\sim 30\%$ at T_N and to slowly increase again with increasing temperature, and up to $6T_N$ strong antiferromagnetic correlations are found to persist. This behavior is consistent with recent theories for itinerant-electron magnetism.

I. INTRODUCTION

It has been of major interest to achieve a unified picture of magnetism for many years.[1,2] The behavior of purely localized magnetic systems, such as magnetic insulators (e.g., MnF_2), and the rare-earth metals is quite well understood in terms of exchange interactions between the localized electrons from each magnetic ion, while another group of magnetic materials (e.g., MnSi) is well described by the theory of weak itinerant-electron magnetism.[1] Here the magnetic moment is entirely supplied by the electrons in the conduction band not localized at specific ions. Although the fully localized and the weak itinerant models describe many magnetic materials, there is still a large group of compounds which is located between the two extremes (e.g., Fe, Ni, and Fe_3Pt), and there are at present no well established theories to describe this group.

The cubic Laves phase intermetallic compound YMn_2 was recently discovered[3] to order antiferromagnetically below $T_N \approx 100$ K. The amplitude of the magnetic moment per Mn atom was determined by this experiment to be $2.7\mu_B$ corresponding to the spin $S=1.35$. For comparison the spin of the free Mn^{2+} ion is $S=\frac{5}{2}$ as it is measured in MnF_2. In the paramagnetic phase above T_N, however, susceptibility[4] and NMR relaxation[5] measurements are similar to those of weak itinerant electron magnets, and this is incompatible with the relatively large localized moment observed in the ordered phase. Also a significant change in lattice constant of $\sim 1.6\%$ with a large thermal hysteresis was observed[4] at T_N. The susceptibility $\chi(0)$ as a function of temperature measured by Shiga *et al.* is shown in Fig. 1. Note that $\chi(0)$ *increases* with increasing temperature. Since most localized magnetic systems for T well above T_c (or T_N) may be considered as ideal paramagnets where the Curie-Weiss law, $\chi(0) \propto M^2/(T-\Theta)$, is valid, an increasing susceptibility for $T \gg T_c$ indicates that the moment M also increases with temperature. This consideration, however, is only valid for an *ideal* (uncorrelated) paramagnet. To investigate magnetic correlations a neutron scattering experiment is a powerful tool and the magnetic moment may be determined directly by this method.[6] Preliminary results[7] have shown that strong magnetic correlations still persist in YMn_2 at room temperature, $T \approx 3T_N$, and indicated a significant decrease in the value of S above the Néel temperature compared to the value in the ordered phase. The observed anomalies and the preliminary neutron scattering results therefore suggest the occurrence of a transition from dominantly local moment magnetism in the low-temperature phase to weak itinerant-electron magnetism in the high-temperature phase, i.e., a change of the electronic state may take place at T_N causing the magnetic moment in YMn_2 to collapse. YMn_2 may therefore provide a unique model system to study in the aim of achieving a unified picture of metal magnetism.

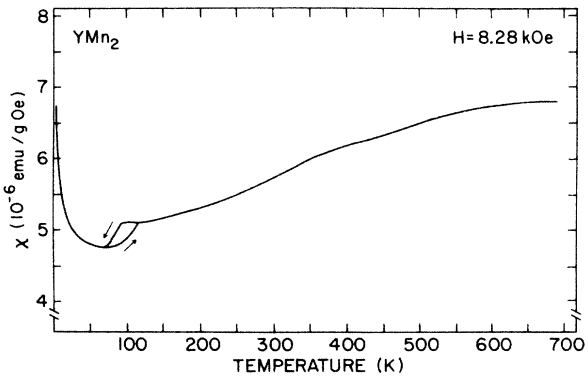

FIG. 1. Temperature dependence of susceptibility of YMn_2 for cooling and heating. After Shiga *et al.* (Ref. 4).

Similar work in the study of paramagnetic neutron scattering from itinerant electron magnets was done by Brown *et al.*[8] on α-Mn. They find a temperature-dependent amplitude of spin fluctuations increasing with increasing temperature between T_N and $3T_N$, but decreasing again between $3T_N$ and $6T_N$. However, an explicit energy integration over the paramagnetic response was not performed in this experiment apart from the integration automatically done by the instrumental resolution.

In the present paper we report a detailed neutron scattering study of a powder sample of YMn_2 using polarized beam analysis of the magnetic response in the ordered phase ($T=10$ K), above the transition at $T\approx 1.5T_N$, $T\approx 3T_N$, and at very high temperature, $T\approx 6T_N$. At each temperature, energy scans are performed in order to estimate the integrated intensity at different Q values, and the procedure used in the powder-data analysis is tested against a well characterized powder sample of MnF_2, where the spin is constant $S=\frac{5}{2}$ independent of temperature.

II. EXPERIMENTAL PROCEDURE

A. Sample preparation

YMn_2 crystallizes in the cubic Cu_2Mg structure [space group ($Fd\bar{3}m$)] with the lattice constant $a=7.68$ Å at room temperature. There are 8 formula units per unit cell, with 8 Y atoms in positions 8(a): fcc$^+$ $\frac{1}{8}\frac{1}{8}\frac{1}{8}$; $\frac{7}{8}\frac{3}{8}\frac{3}{8}$; and 16 Mn atoms in positions 16(d): fcc$^+$ $\frac{1}{2}\frac{1}{2}\frac{1}{2}$; $\frac{1}{4}\frac{3}{4}0$; $0\frac{1}{4}\frac{3}{4}$; $\frac{3}{4}0\frac{1}{4}$; the powder sample was prepared by melting Y and Mn metals in an argon arc furnace. The purity of the component metals is 99.9% and the 0.1% impurities are mainly Au, La, and Ta. The ratio of Y and Mn atoms was Y/Mn=1.05/2.00; the excess amount of Y was added to avoid formation of Mn rich ferromagnetic compounds such as Y_6Mn_{23}. The ingot was annealed at 800 °C for one week and then crushed into powder. Approximately 23 g of the sample kept in He atmosphere to avoid oxidation was loaded into a 2.5 cm high and 1.9 cm diameter cylindrical aluminum container and sealed with indium for the low-temperature measurements. For the high-temperature experiment 28 g of YMn_2 powder was loaded into a 3.7 cm high and 1.9 cm diameter cylindrical aluminum holder which was electron beam sealed in vacuum. Temperatures up to 594 K were reached using a pumped aluminum shielded air cooled furnace.

We checked the magnetic structure and moment in the ordered phase at $T=10$ K. In Fig. 2 the powder spectrum is shown together with the peak intensity of the strongest magnetic reflection as a function of temperature showing that the transition is of first order. Our measurement confirms the arrangement of up and down spins (see Fig. 3) found by Nakamura *et al.*[3] The spin direction is found to be $\phi=55°$ from the magnetic tetragonal axis and the spin is $S=1.41\pm0.05$ in good agreement with Nakamura's result which corresponds to $S=1.35$. Note that the form of the magnetization curve in the inset of Fig. 2 indicates that S does not change with temperature in the ordered phase.

B. Polarized-beam measurements

A very direct method of eliminating the nuclear background and isolating the magnetic scattering from a sample is to perform a polarized neutron scattering experiment, although, the method has the disadvantage of very low signal rates, which requires some compromises in resolution and counting times.

The measurements were made on a modified triple-axis spectrometer using vertically magnetized Heusler (111) transmission crystals at the monochromator and analyzer positions. Magnetic guide fields were used along the beam path to maintain the polarization of the neutrons, and a flipping coil was placed between the sample and analyzer. A weak magnetic field was applied at the sample position to orient the neutron polarization either along the scattering vector, Q (horizontal field, HF) or perpendicular to Q (vertical field, VF). Inelastic spectra were measured at constant Q with a fixed final energy of either 41 or 60 meV and collimations of 40′-80′-80′-130′, providing energy resolutions at $\omega=0$ of about 10 and 17 meV full width at half maximum (FWHM) respectively. The overall flipping ratio R of the instrument was $R=15$ or better for both HF and VF, and the relative difference in R measured for HF and VF was less than 5%. The flipping ratio, which is the ratio of spin-flip to non-spin-flip events, was optimized using the (002) reflection of a pyrolytic graphite (PG) crystal at the sample position and

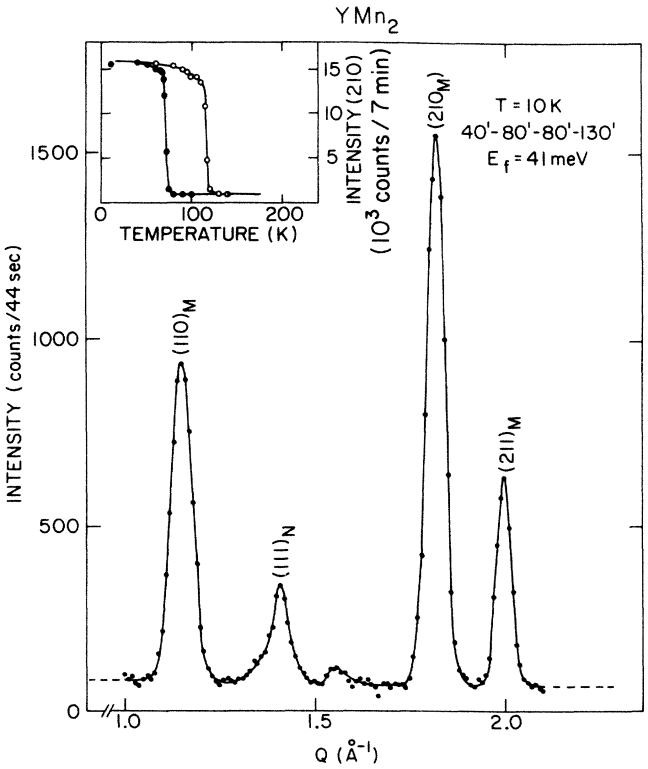

FIG. 2. Neutron diffraction spectrum from YMn_2 powder sample in the ordered phase taken with flipper on and a horizontal magnetic field at the sample position. The inset shows the peak intensity of the (210) magnetic Bragg peak as a function of temperature.

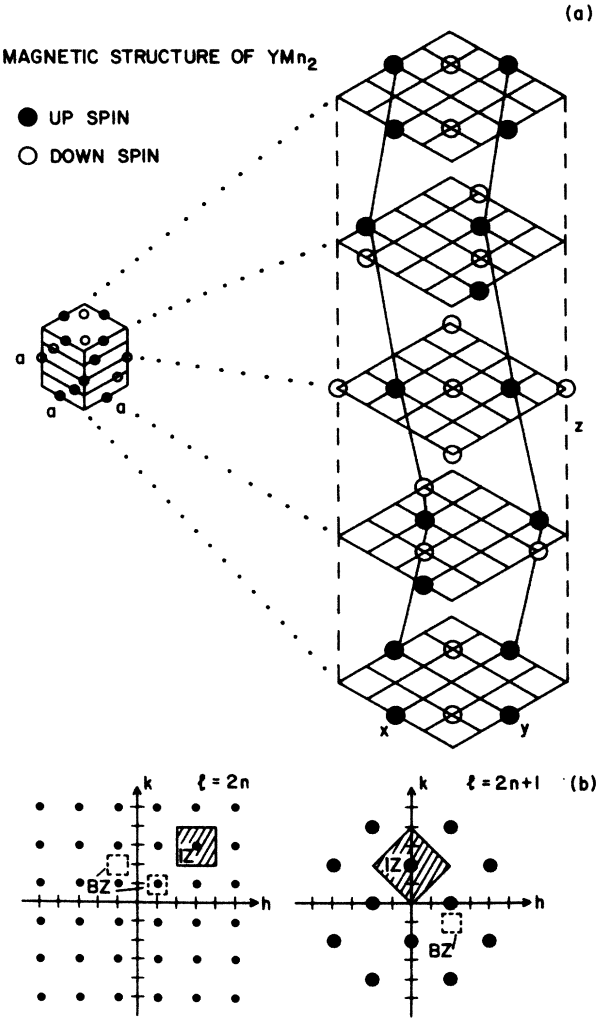

FIG. 3. (a): The assumed magnetic structure of YMn_2. Only the Mn atoms are shown. Open and closed circles represent spin up and spin down, respectively. The spin direction is 55° off the c axis which is vertical in the figure. (b): Corresponding magnetic structure factor regardless of spin direction. The reflections in the $l=2n$ planes (small dots) have half the intensity compared to the reflections in the $l=2n+1$ planes (large dots). The definitions of intensity zones (Ref. 11) (IZ) and Brillouin zone (BZ) are indicated.

with a PG filter to avoid higher-order contamination of the beam in the optimization procedure. However, in order to achieve a reasonable neutron count rate from the YMn_2 sample no filters were used in this case to attenuate higher-order contaminations. But since the guide field and flipper currents were tuned to optimize the flipping ratio only for the first-order initial energy, the higher-order contributions will appear mainly as depolarized background. This is consistent with the fact that no higher-order peaks were observed in the powder spectra.

In Table I we review the cross sections[9] in the four possible combinations of flipper on/off and HF/VF. As may be seen, the difference HF-VF and flipper on yields $\frac{1}{2}$ of the magnetic cross section measured in the unpolarized neutron scattering experiment, and the contributions from background and nuclear-spin incoherent scattering cancel.

TABLE I. Magnetic σ_M and nuclear σ_N neutron cross sections for the polarization analysis setup. E_f is fixed and the flipper is placed after the sample. $\sigma_{\rm NSI}$ is nuclear spin incoherent cross section and bg is background.

	Flipper on (+/−)	Flipper off (+/+)
Horizontal field	$\sigma_M+\frac{2}{3}\sigma_{\rm NSI}+bg$	$\sigma_N+\frac{1}{3}\sigma_{\rm NSI}+bg'$
Vertical field	$\frac{1}{2}\sigma_M+\frac{2}{3}\sigma_{\rm NSI}+bg$	$\sigma_N+\frac{1}{2}\sigma_M+\frac{1}{3}\sigma_{\rm NSI}+bg'$

III. RESULTS AND ANALYSIS

Figure 4 shows inelastic polarized beam measurements of YMn_2 powder for constant wave vector $Q=1.8$ Å^{-1} and $Q=2.1$ Å^{-1} at three different temperatures, 150, 293, and 594 K. The data were taken with flipper on and (HF-VF) as explained in Sec. II. Correction for misalignment of the horizontal field direction with the scattering vector for $E\neq 0$ has been applied. It can be seen that the energy width Γ apparently is temperature dependent at $Q=1.8$ Å^{-1}, but not for $Q=2.1$ Å^{-1}. This behavior may be caused by the powder averaging as will be explained later.

In Fig. 5 the wave vector dependence for zero energy transfer is shown for the same temperatures, and also the cross sections calculated from susceptibility measurements are plotted at $Q=0$. The broad peak observed centered around $Q\approx 1.8$ Å^{-1}, which is the position of the strongest magnetic Bragg peak in the antiferromagnetically ordered phase, indicates that the persisting correlations above T_N are of antiferromagnetic nature. Note that the correlations are still significant at $T=594$ K$\approx 6T_N$. For comparison the cross sections of an ideal paramagnet with spin $S=1$ is also shown in Fig. 5. This cross section is simply proportional to the magnetic formfactor squared $f^2(Q)$ and here again the Mn^{2+} formfactor is assumed.

Cross sections in absolute scale may be obtained by integrating the measured intensities over energy and normalizing to a nuclear Bragg peak. The energy integration is explained below and the entire procedure has been described in detail by Goldman *et al.*[10] So far, there is no first-principles theory of the paramagnetic scattering from 3*d* transition compounds to be compared with the experimental results. However, it has been demonstrated that for a *single crystal* the cross section may be expressed

$$\frac{d^2\sigma}{d\omega\, d\Omega}=\gamma_0^2 f^2(Q)e^{-2W}S(q,\omega)\ . \tag{1}$$

$Q=4\pi/\lambda\sin\theta$ is the scattering vector measured with respect to the direct beam and q the wave vector relative to the peak position, e^{-2W} the Debye-Waller factor. Close to a diffuse peak

$$S(q,\omega)=\tfrac{1}{6}M^2(q)\frac{1}{\pi}\frac{\Gamma}{\Gamma^2+\omega^2}\frac{\hbar\omega/kT}{1-e^{-\hbar\omega/kT}} \quad (2)$$

to a first approximation with

$$M^2(q)=M^2(0)\frac{\kappa_1^2}{\kappa_1^2+q^2}\ . \quad (3)$$

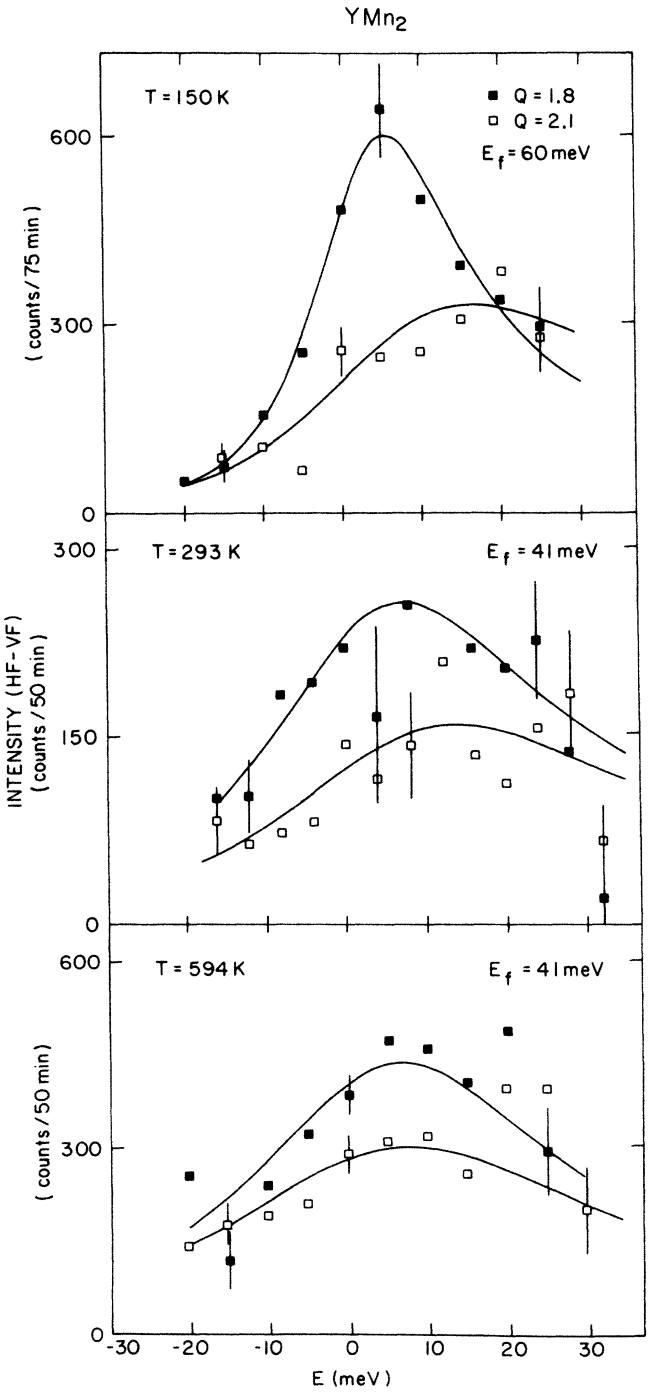

FIG. 4. Paramagnetic scattering spectra obtained using the parallel-perpendicular method (HF-VF). The curves are fits of Lorentzian lineshapes to the data (including the detailed balance correction).

Γ is the energy linewidth and κ_1 the inverse correlation length. The spin S may then be calculated from $M^2(q)$ by averaging over the intensity zone (IZ) (Ref. 11)

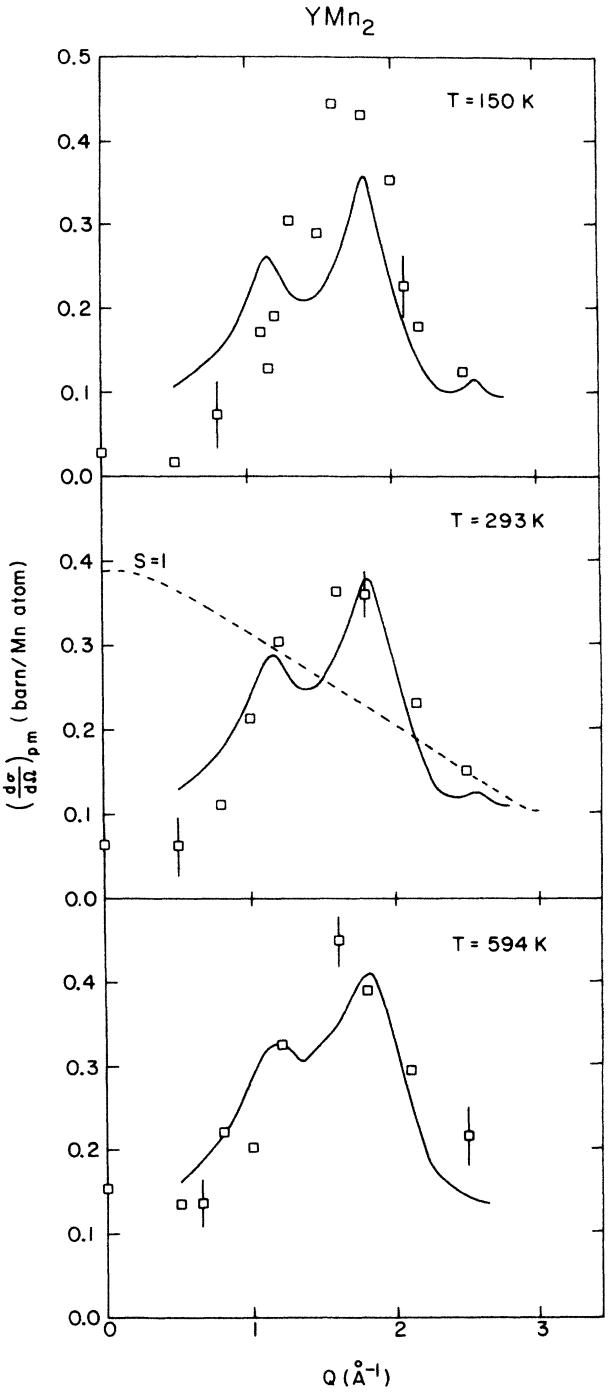

FIG. 5. Energy integrated cross sections as a function of momentum transfer. The absolute scale is obtained by normalizing to a nuclear Bragg peak and the points shown for $Q=0$ are calculated from susceptibility data. Model calculations of the powder average which best fitted the data are shown as solid curves. The values for the magnetic moment obtained this way are shown in Fig. 6. The dashed curve corresponds to the cross section calculated for an *ideal* paramagnet with spin $S=1$ for comparison.

$$4S(S+1)=\frac{1}{V_{IZ}}\int_{IZ}M^2(q)d^3q \ . \quad (4)$$

To extract $M^2(q)$ from the measured intensities in Figs. 4 and 5 we first note that from Eq. (2)

$$M^2(q)=6\int_{-\infty}^{\infty}\frac{1-e^{-\hbar\omega/kT}}{\hbar\omega/kT}S(q,\omega)d\omega \quad (5)$$

i.e., after removing the thermal factor the measured $S(q,\omega)$ is integrated over ω. As may be seen from Fig. 4, the constant Q scans do not cover more than the range from -20 to 20 meV due to instrumental limitations. In order to estimate the fully energy integrated intensity a Lorentzian is fitted to the data in Fig. 4 after removal of the thermal factor, and the missing intensity from the tails is added to the sum of the measured points. Assuming a Lorentzian lineshape over the entire energy range is considered an upper limit for the absolute cross section, and hence, also for the moment. The energy window actually accessed by the present experiment corresponds to $\sim 2\Gamma$ which for a Lorentzian covers approximately half of the fully integrated response. Integrating only over this window would heavily underestimate the derived moment, so as a compromise the lower limit of the integrated intensity is assumed to be $\frac{3}{4}$ of the full Lorentzian integration.

For a Heisenberg antiferromagnet Γ is expected to depend on q as $\Gamma\sim q^{1.5}$ for small q,[12] but not to be strongly dependent of temperature,[13] i.e., the line width is narrow close to the IZ center. Now, the present data are from a powder sample, and hence, the observed cross section represents contributions from different diffuse peaks (i.e., several IZ's). Therefore, the observed energy width represents some average. For $T=150$ K where κ_1 is still relatively small (~ 0.1 Å^{-1}), this average is not independent of Q, since contributions very close to a zone center where Γ is small are weighed much stronger than contributions from more distant peaks. This is the reason why Γ is observed to vary significantly with Q for $T=150$ K, but not for the higher temperatures. Ideally, constant Q scans should have been taken for all Q values considered, but this was not possible due to instrumental limitations. In the analysis of the $T=293$ and 594 K data, the average Γ obtained for $Q=1.8$ Å^{-1} and $Q=2.1$ Å^{-1} from each temperature was used for the energy integration of all data points. In the case of $T=150$ K only the value of Γ for $Q=2.1$ Å^{-1} was used since it represents a better average than the value observed for $Q=1.8$ Å^{-1}.

As mentioned, the present data are from a powder sample, and so, the measured $M^2(Q)$ contains contributions from several IZs. Therefore, $M^2(q)$ In Eq. (2) should be replaced by a powder average $M^2_{av}(Q)$

$$M^2_{av}(Q)=\frac{1}{4\pi Q^2}\sum_{hkl}\int_{S_Q}M^2(q_{hkl})dS \ . \quad (6)$$

S_Q is the part of a spherical shell with radius Q in Q space which intersects a given IZ(hkl). Note the difference between q which is the scattering vector relative to the magnetic Bragg peak (hkl) below T_N, and Q which is the scattering vector with respect to the forward direction. Details of a computer program calculating this powder average will be given in the Appendix.

As may be seen from Eqs. (2)–(6) the powder average can be calculated using only two parameters $M^2(0)$ and κ_1, and in Table II the values from least-squares fits to the data of Fig. 5 are shown. Also the values of the spin S calculated from Eq. (4) using the fitted values of $M^2(0)$ and κ_1 are shown in the table. The integration over the IZ was performed as a simple average over a sphere with the same volume as the actual IZ. The shape of the fitted curves is in reasonable agreement with the data, best for the higher temperatures. The inconsistency at 150 K reflects the limitations of the very simple model assumed [Eq. (3)]. More sophisticated models taking into account possible deviations from the Lorentzian in Eq. (3) near the zone boundary or nonhomogeneous distribution of moments on the Mn atoms in the unit cell would provide better agreement with the observed data. However, the introduction of additional unknown parameters is not justified by the statistical accuracy of the powder data. A single crystal is required to obtain detailed information concerning these features.

A crude estimate of the magnetic moment in a paramagnetic scatterer may be calculated by simply integrating the measured cross sections over Q (taking into account the volume factor $4\pi Q^2$) and comparing it to the integrated cross section for the ideal paramagnet.[7] The crude estimates of S obtained by this method are also given in Table II and are seen within error to be in agreement with the values derived by the model calculations. In Fig. 6 the deduced spin S is plotted as a function of temperature; the moment is seen to "collapse" around T_N and increase again with increasing temperature above T_N. The squares shown above T_N correspond to the upper limit established by the full energy integration assuming Lorentzian line shape from $-\infty$ to $+\infty$.

IV. DISCUSSION

Let us first summarize our experimental observations for YMn_2. In the antiferromagnetically ordered phase

TABLE II. Energy linewidth Γ, inverse correlation length κ_1, and $M^2(q=0)$ obtained from YMn_2 powder data. S (powder average) is calculated from κ_1, and $M^2(0)$ by averaging over the intensity zone. S (crude) is estimated from integrating the data in Fig. 5 directly.

T/(K)	$\Gamma(Q=1.8)$ (meV)	$\Gamma(Q=2.1)$ (meV)	κ_1 (Å^{-1})	$M^2(q=0)$ (μ_B)	S (powder average)	S (crude)
150	12±1	24±3	0.10	157±8	0.85±0.03	0.9±0.2
293	22±3	27±6	0.13	123±6	0.94±0.03	1.0±0.2
594	24±2	28±5	0.17	89±4	1.04±0.03	1.2±0.2

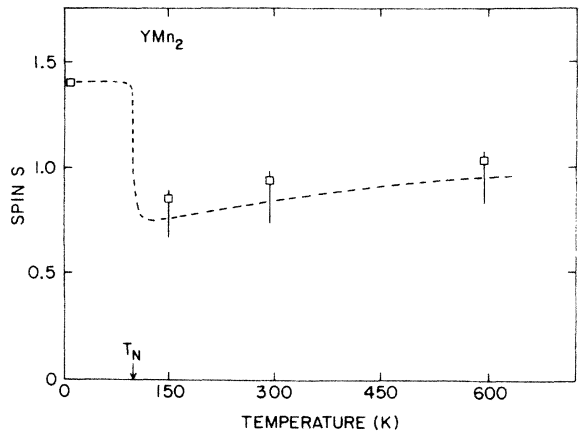

FIG. 6. Local amplitude S of spin fluctuations per Mn atom as a function of temperature. The line is a guide to the eye.

the moment per Mn atom is determined to $S=1.4$. This relatively large value is interpreted as indicating a predominantly local moment system, although the spin of the free Mn^{2+} ion is $S=\frac{5}{2}$. At present, there is no direct method to verify this interpretation. As the temperature is increased to $T\approx 100$ K a change in the electronic state causes a collapse of the moment to $S\approx 0.8$ and the system becomes paramagnetic.

In the paramagnetic phase we observe strong antiferromagnetic correlations at least up to $6T_N$. The inverse correlation length κ_1 deduced from powder average fits, increases only by a factor of approximately 2 between 1.5 and $6T_N$. However, the absolute value of κ_1 is not very well determined due to the limitations provided by a powder sample. A single crystal of YMn_2 is needed in order to investigate the temperature dependence of κ_1 in detail, but so far, no attempts to grow a crystal have succeeded.

In the paramagnetic region the local amplitude of the spin fluctuations S is observed to increase slightly with increasing temperature. Both the persisting correlations and this increase in S are in qualitative agreement with Moriya's theory of weak itinerant magnetism,[2] although this theory has mainly been applied to systems with even smaller moment than $S=0.8$, e.g., Ni_3Al where $S=0.038$;[14] but also MnSi where $S=0.5$ has been found to comply with the theory.[15]

In conclusion we note that to fully understand the behavior of metallic magnetic systems a unified theory combining local moment and weak itinerant magnetism is required, and we hope that the present results may stimulate the development of such a theory.

ACKNOWLEDGMENTS

We are grateful for stimulating discussions with Professor M. Shiga and Dr. A. I. Goldman. This work was carried out as a part of the U.S.-Japan Cooperative Neutron Scattering Program. The work at Brookhaven National Laboratory was supported by the Division of Materials Sciences, U.S. Department of Energy under Contract No. DE-AC02-76CH00016.

APPENDIX

In this appendix we show the details of the powder average used in the analysis of data taken in the paramagnetic regime above T_N. The assumptions used may be summarized as follows:

(1) The sample is considered to be an ideal powder, i.e., all crystallites have completely random orientations.

(2) The reciprocal space of a crystallite is divided into intensity zones (IZ's) (Ref. 11) centered around each original magnetic Bragg peak. The extent of an IZ is defined so that a general point in Q space belongs to the IZ centered around the nearest Bragg position. See Fig. 3(b) for the definition of IZ's in YMn_2.

(3) At the position of each original magnetic Bragg peak a diffuse Lorentzian peak of the form Eq. (3) is assumed extending to the IZ boundary. The relative amplitudes of the peaks are scaled according to the magnetic structure factors.

The powder average for a specific Q is now calculated by considering a spherical shell of radius Q in the reciprocal space of a crystallite. The surface of this shell is subdivided into a large number (800) of small pixels, and for each pixel the appropriate IZ is determined. The distance q_{hkl} to the IZ center is calculated and the scattering from the pixel is found as given by Eq. (3). Contributions from all pixels are then summed and divided by $4\pi Q^2$ to obtain the powder average $M^2_{\rm av}(Q)$ in Eq. (6).

[1]T. Moriya, *Spin Fluctuations in Itinerant Electron Magnetism* (Springer, Berlin, 1985).

[2]T. Moriya, J. Magn. Magn. Mater. **14**, 1 (1979).

[3]Y. Nakamura, M. Shiga, and S. Kawano, Physica **120B**, 212 (1983).

[4]M. Shiga, H. Wada, and Y. Nakamura, J. Magn. Magn. Mater. **31-34**, 119 (1983).

[5]K. Yoshimura, M. Takigawa, H. Yasuoka, M. Shiga, and Y. Nakamura, J. Magn. Magn. Mater. **54-57**, 1075 (1986).

[6]G. Shirane, Physica **137B**, 43 (1986).

[7]K. Motoya, T. Freltoft, P. Böni, and G. Shirane, J. Phys. Soc. Jpn. **56**, 885 (1987).

[8]P. J. Brown, K. R. A. Ziebeck, J. G. Booth, and H. Capellmann, Z. Phys. B **50**, 223 (1983).

[9]R. M. Moon, T. Riste, and W. C. Koehler, Phys. Rev. **181**, 920 (1969).

[10]A. I. Goldman, S. M. Shapiro, G. Shirane, J. L. Smith, and Z. Fisk, Phys. Rev. B **33**, 1627 (1986).

[11]We define intensity zones (IZ) in reciprocal space as the unit over which the structure factor repeats, and they are centered where this has a local maximum corresponding to the position of a magnetic Bragg peak in the ordered phase. In the simple case of a structure with only one atom per unit cell IZs are equivalent to Brillouin zones (BZs). For more complex structures (e.g. YMn_2) IZs are generally larger than BZs, and may be of different volumes depending on the reflection around which they are centered. In Fig. 3(b) the reciprocal lattice for YMn_2 is shown together with examples of the two

different size IZs which exist in this structure. Also shown are examples of BZs.

[12]B. I. Halperin and P. C. Hohenberg, Phys. Rev. **177**, 952 (1969).

[13]P. Résibois and C. Piette, Phys. Rev. Lett. **24**, 514 (1970).

[14]G. G. Lonzarich, J. Magn. Magn. Mater. **45**, 43 (1984).

[15]Y. Ishikawa, Y. Noda, Y. J. Uemura, C. F. Majkrzak, and G. Shirane, Phys. Rev. B **31**, 5884 (1985).